

Ab initio calculation of structural and electronic properties of $\text{Al}_x\text{Ga}_{1-x}\text{N}$ and $\text{In}_x\text{Ga}_{1-x}\text{N}$ alloys

E. López-Apreza^a, J. Arriaga^a, and D. Olgún^b

^a*Instituto de Física, Universidad Autónoma de Puebla, Apartado Postal J-48, Puebla, 72570, México.*

^b*Departamento de Física, Centro de Investigación y de Estudios Avanzados del Instituto Politécnico Nacional, Apartado Postal 14740, México, 07300, D.F., México.*

Recibido el 25 de febrero de 2010; aceptado el 5 de mayo de 2010

Using the density functional theory (DFT) with the generalized gradient approximation (GGA), we calculated the structural and electronic properties of wurtzite AlN, GaN, InN, and their related alloys, $\text{Al}_x\text{Ga}_{1-x}\text{N}$ and $\text{In}_x\text{Ga}_{1-x}\text{N}$. We have performed accurate *ab initio* total energy calculations using the full-potential linearized augmented plane wave (FP-LAPW) method to investigate their structural and electronic properties. We found that in both alloys the fundamental parameters do not follow Vegard's law. The lattice parameters, a , c , and u , for the $\text{Al}_x\text{Ga}_{1-x}\text{N}$ alloy are found to exhibit positive bowing parameters, while for $\text{In}_x\text{Ga}_{1-x}\text{N}$ there is a negative bowing for the a and c parameters and a positive bowing for the internal parameter, u . We calculated as well the nearest neighbor and next nearest neighbor distances, as a function of the concentration, and we obtained a good agreement with experimental results. Furthermore, we found that for both alloys, the band gap does not follow the Vegard law. As a by-product of our electronic band structure calculations, the effective masses of the binary compounds and their alloys were calculated. All the calculated properties show good agreement with most of the previously reported results. Finally, using the frozen phonon approach, the $A_1(TO)$ mode for the different systems studied in this work was calculated. Our calculations show good agreement with experimental values reported for the binary compounds. For the ternary alloys, our calculations reproduce experimental values for $\text{Al}_x\text{Ga}_{1-x}\text{N}$ as well as theoretical predictions for $\text{In}_x\text{Ga}_{1-x}\text{N}$.

Keywords: *Ab initio* calculations; nitride semiconductor alloys.

Calculamos las propiedades estructurales y electrónicas de los compuestos AlN, GaN, InN y sus aleaciones ternarias $\text{Ga}_{1-x}\text{Al}_x\text{N}$ y $\text{Ga}_{1-x}\text{In}_x\text{N}$ usando la teoría del funcional de la densidad (DFT) dentro de la aproximación del gradiente generalizado (GGA). Para el estudio de las propiedades electrónicas y estructurales hemos realizado cálculos de energía total usando el método de ondas planas generalizadas. En nuestro estudio hallamos que los parámetros fundamentales de estas aleaciones no obedecen la ley de Vegard. Encontramos que para la aleación $\text{Al}_x\text{Ga}_{1-x}\text{N}$, los parámetros de red a , c y u muestran un parámetro de arqueo positivo. Para la aleación $\text{In}_x\text{Ga}_{1-x}\text{N}$ sus parámetros a y c muestran un parámetro de arqueo negativo, mientras que su parámetro interno u posee un parámetro de arqueo positivo. Calculamos también las distancias a primeros y segundos vecinos de las aleaciones, las cuales se comparan muy bien con resultados experimentales. Encontramos que para ambas aleaciones la brecha de energía prohibida, como función de la composición, no muestra un comportamiento lineal. Adicionalmente a los cálculos de estructura electrónica, calculamos también las masas efectivas tanto para los compuestos binarios como para las aleaciones. Mostramos que las propiedades calculadas en este trabajo muestran un buen acuerdo con la mayoría de los resultados reportados anteriormente. Finalmente, usando la aproximación del “fonón congelado”, calculamos el modo $A_1(TO)$ para todos los sistemas estudiados. Nuestros resultados muestran un buen acuerdo con los resultados experimentales reportados para los compuestos binarios. Para las aleaciones, nuestros cálculos reproducen tanto los resultados experimentales para $\text{Al}_x\text{Ga}_{1-x}\text{N}$ así como las predicciones teóricas de la aleación $\text{In}_x\text{Ga}_{1-x}\text{N}$.

Descriptores: Cálculos *Ab initio*; aleaciones de nitruros.

PACS: 71.15.Mb; 71.20.Nr; 71.20.-b

1. Introduction

The III–Nitride semiconductors have attracted much attention over recent years because of their potential applications in technological devices. This is due mainly to the fact that the energy gap can be tuned over a wide spectral range from the visible to the ultraviolet regime of the electromagnetic spectrum. Although the zincblende and wurtzite structures are present in the GaN, AlN, and InN semiconductors, it has been demonstrated experimentally that wurtzite is the most stable structural phase of these compounds. Moreover, due to their high chemical and thermal stability, the III–Nitrides are ideal candidates for applications under extreme conditions such as high temperature applications. In the wurtzite crys-

talline structure the value of the band gap ranges from 0.8 eV for InN [1], 3.4 eV for GaN [2] and 6.2 eV for AlN [3], providing a huge interval of energies for this parameter whenever the concentration forming the alloy is carefully selected. The hexagonal wurtzite structure is extensively utilized because all the III–nitride semiconductors and their alloys exhibit a direct band gap energy, which results in a high emitting performance [4,5]. Due to the remarkable progress in epitaxial growth technology, high quality samples of these compounds can be produced. High-quality wurtzite InN is currently available and its direct band gap energy has been determined to be between 0.7 and 0.8 eV, which is much smaller than the first accepted value of 1.9 eV [1,6]. From a theoretical point of view, many calculations using different

methods have been done to characterize the structural, electronic, and optical properties of these systems; however there is still no agreement in the scientific community concerning the values of certain parameters, since they show significant scattering when we compare the experimental or theoretical results published in the literature.

In this paper, by means of numerical calculations based on first principles, we present a study of the structural and electronic properties of the wurzite structure AlN, GaN, InN semiconductors and their related alloys, $\text{Al}_x\text{Ga}_{1-x}\text{N}$ and $\text{In}_x\text{Ga}_{1-x}\text{N}$. The analysis was made by calculating the total energy. First, we analyzed the binary compounds, GaN, AlN, and InN, and then their related alloys, $\text{Al}_x\text{Ga}_{1-x}\text{N}$ and $\text{In}_x\text{Ga}_{1-x}\text{N}$. Our calculations were based on the density functional theory (DFT) using the generalized gradient approximation (GGA) in order to calculate the exchange-correlation term in the total energy. We used the Wien2k simulation package developed by the Vienna University of Technology. In Sec. 2, we describe the model used in this work, while in Sec. 3, we discuss our results and compare them with the data found in the literature. Finally, in Sec. 4, we present our conclusions.

2. Theoretical aspects and computational method

Our calculations were performed within the framework of the density functional theory (DFT) [7], which states that all the ground state properties of a system are functionals of the electron density, and the total energy is expressed in terms of the electron density rather than the wave function. At present, DFT is one of the most accurate methods for calculating the structural and electronic properties of solids. We have used the full-potential linearized augmented plane wave method (FP-LAPW) as implemented in the Wien2k code [8]. As most of the first principles methods, LAPW is a procedure used to solve the Khon-Sham set of equations for the density of the ground state, the total energy, and the eigenvalues of a many-electron system. In the present analysis, the exchange-correlation energy of the electrons was treated using the generalized gradient approximation (GGA), in the scheme proposed by Perdew, Burke, and Ernzerhof [9]. To minimize the energy, the Wien2k code divides the unit cell into non-overlapping spheres centered at atomic sites (muffin-tin (MT) spheres), and the interstitial region. In the MT spheres, the Khon-Sham orbitals are expanded as a linear product of radial functions and spherical harmonics, and as a plane wave

TABLE I. Structural parameters for the AlN, GaN, and $\text{Al}_x\text{Ga}_{1-x}\text{N}$ alloys. The lattice parameters a and c are given in Å.

System	Parameter	This Work	Exp. Results	Other Calc.
GaN	a	3.2209	3.1890 ^a , 3.1892 ^b 3.1880 ^f , 3.19 ^g	3.1660 ^c , 3.189 ^d , 3.2 ^e 3.1800 ^h , 3.1986 ⁱ , 3.17 ^j , 3.183 ^k
	c	5.2368	5.1850 ^a , 5.185 ^b 5.18561 ^f , 5.189 ^g	5.1540 ^c , 5.185 ^d , 5.2200 ^e 5.1898 ^h , 5.2262 ⁱ , 5.151 ^j , 5.178 ^k
	u	0.3780	0.3768 ^a , 0.377 ^g	0.3770 ^c , 0.3768 ^d , 0.3760 ^e 0.3760 ^h , 0.3772 ⁱ , 0.3768 ^j
$\text{Al}_{0.25}\text{Ga}_{0.75}\text{N}$	a	3.2059	See Ref. 11 and 12	3.163 ^k
	c	5.1338		5.137 ^k
	u	0.3781		
$\text{Al}_{0.50}\text{Ga}_{0.50}\text{N}$	a	3.1719	See Ref. 11 and 12	3.139 ^k
	c	5.1012		5.085 ^k
	u	0.3790		
$\text{Al}_{0.75}\text{Ga}_{0.25}\text{N}$	a	3.1601		3.098 ^k
	c	5.0870	See Ref. 11 and 12	4.990 ^k
	u	0.3791		
AlN	a	3.1411	3.1120 ^a , 3.11 ^g 3.1106 ^l	3.0920 ^c , 3.084 ^d , 3.1 ^e 3.0610 ^h , 3.10954 ⁱ , 3.098 ^j , 3.076 ^k
	c	5.0268	4.9820 ^a , 4.98 ^g 4.9795 ^l	4.954 ^c , 4.9948 ^d , 5.010 ^e 4.8976 ^h , 4.9939 ⁱ , 4.9599 ^j , 4.935 ^k
	u	0.3805	0.3819 ^a , 0.3821 ^g	0.3821 ^c , 0.3814 ^d , 0.3800 ^e 0.3820 ^h , 0.3819 ⁱ , 0.3819 ^j

^a Ref. 28 S. Strite *et al.*, ^b Ref. 29 T. Detchprohm *et al.*, ^c Ref. 15 Z. Dridi *et al.*, ^d Ref. 33 A.F. Wright *et al.*, ^e Ref. 34 C. Bungaro *et al.*,

^f Ref. 30 M. Leszczynski *et al.*, ^g Ref. 31 H. Schulz *et al.*, ^h Ref. 21 J. Serrano *et al.*, ⁱ Ref. 23 A. Zoroddu *et al.*, ^j Ref. 24 P. Carrier *et al.*,

^k Ref. 16 B.T. Liou *et al.*, ^l Ref. 32 M. Tanaka *et al.*

expansion in the interstitial region. The basis set inside each MT sphere is divided into core and valence subsets. The core states were treated fully relativistically, whereas a scalar scheme was used for the valence states. No spin-orbit splitting was included in our calculations. The core states are treated within the spherical part of the potential only and are assumed to have a spherically symmetric charge density completely confined within the MT spheres. In this work, the valence part was treated as a potential, and was expanded into harmonics up to $l = 10$. We have used MT sphere radii, in a. u., of 1.6 for N, 1.9 for Al, 2.0 for Ga, and 2.33 for In. The self-consistent calculation was considered to converge when the total energy of the system was stable within 10^{-5} Ry. Care was taken to assure the convergence of the total energy in terms of the variational cutoff energy parameter. Furthermore, we have used an appropriate set of k-points to compute the total energy. To calculate the convergence of the total energy we wrote the basis functions up to a cutoff radius of $R_{mt}K_{max} = 7$ Ry for both the binary compounds and the $\text{Al}_x\text{Ga}_{1-x}\text{N}$ alloy and a cutoff radius of $R_{mt}K_{max} = 8$ Ry for the $\text{In}_x\text{Ga}_{1-x}\text{N}$ alloy. The chosen values for $R_{mt}K_{max}$ assure the convergence of the total energy up to 10^{-5} Ry in all the studied systems. Then, we minimized the total energy using different sets of k-points in the irreducible part of the Brillouin zone and constructing an appropriate grid mesh in the unit cell according to the Monkhorst-Pack procedure [10]. The number of k-points used was chosen in order to assure convergence within our accuracy criterion (10^{-5} Ry). We used a set of 1000 k-points for GaN, 550 for AlN, 630 for InN, 700 for $\text{Al}_{1-x}\text{Ga}_x\text{N}$, and 900 for $\text{In}_{1-x}\text{Ga}_x\text{N}$. In the Monkhorst-Pack scheme these set of k-points are equivalent to $12 \times 12 \times 6$, $10 \times 10 \times 5$, $10 \times 10 \times 5$, and $11 \times 11 \times 6$ grid mesh, respectively.

In the wurtzite structure, the positions of the atoms inside the unit cell are $(0, 0, 0)$ and $(2/3, 1/3, 1/2)$ for the cation (Al, Ga, or In) and $(0, 0, u)$ and $(2/3, 1/3, 1/2 + u)$ for the anion N, where u is the internal parameter for the cation-anion separation. We began our study by optimizing the structural parameters for the binary compounds, GaN, AlN, and InN, starting from the ideal wurtzite structure with a ratio $c/a = 1.633$ and $u = 0.375$ for the internal parameter. This optimization was made by an iterative process as a function of the volume V , the c/a ratio, and the internal parameter u , until the total energy converged within 0.01 mRy. To model the $\text{Al}_x\text{Ga}_{1-x}\text{N}$ and $\text{In}_x\text{Ga}_{1-x}\text{N}$ ternary alloys, we used a 32-atom supercell with periodic boundary conditions. This corresponds to a $2 \times 2 \times 2$ supercell which is twice the size of the primitive wurtzite unit cell in all directions: along the basal plane and along the c -axis. We minimized the total energy for different values of the concentration, x (0.25, 0.50, and 0.75), as a function of the three variables mentioned above. The atomic electronic configurations used in our calculations were: Al (Ne, 3p, 3s), Ga (Ar, 3d, 4s, 4p), In (Kr, 4d, 5s, 5p), and N (He, 2s, 2p). The Ga3d and In4d electrons were treated

as valence band states using the local orbital extension of the LAPW method [8].

3. Results and discussion

3.1. Structural parameters for the $\text{Al}_x\text{Ga}_{1-x}\text{N}$ and $\text{In}_x\text{Ga}_{1-x}\text{N}$ alloys

3.1.1. $\text{Al}_x\text{Ga}_{1-x}\text{N}$

Table I summarizes our calculated structural parameters and compares them with experimental and theoretical results found in the literature. We observed that the values of the lattice parameters for the $\text{Al}_x\text{Ga}_{1-x}\text{N}$ alloy decrease when the Al content is increased. This is due to the fact that the size of the Al atom is smaller than the Ga atom. This is not the case for the internal parameter, u , in which we observe an increase of this parameter when we increase the Al content in the alloy. Figure 1a shows the behavior of the a and c parameters as a function of the Aluminum concentration. We can see from the figure that these parameters show a clear deviation from the linear behavior stated by Vegard's law. The deviation from Vegard's law can be quantified by adjusting the curves in Fig. 1a to the following formula:

$$A(x) = xA_{\text{AlN}} + (1 - x)A_{\text{GaN}} - \epsilon_A x(1 - x), \quad (1)$$

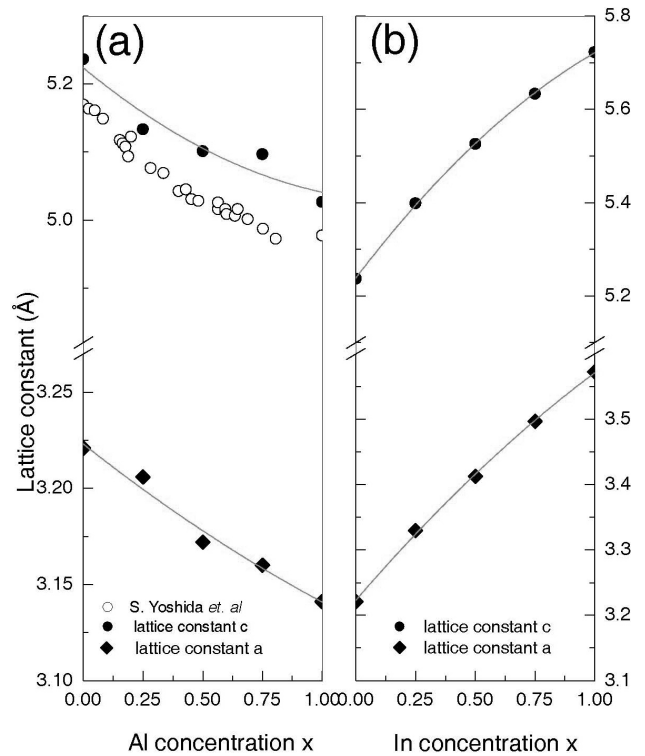


FIGURE 1. (a) Calculated lattice constants a and c for the $\text{Al}_x\text{Ga}_{1-x}\text{N}$ alloy as a function of the Aluminium composition, x . Open circles show the experimental results for the lattice parameter c (after S. Yoshida *et al.* [11]). (b) Calculated lattice constants a and c for the $\text{In}_x\text{Ga}_{1-x}\text{N}$ alloy as a function of the Indium composition, x .

where $A(x)$ stands for the different structural parameters, a , c , and u , of the $\text{Al}_x\text{Ga}_{1-x}\text{N}$ alloy. A_{AlN} (A_{GaN}) represents the structural parameter of the binary AlN (GaN) compound and ϵ_A is the respective bowing parameter. If we fit our calculated values from Table I to Eq. (1), we obtain the following bowing parameters: $\epsilon_a = 0.016 \text{ \AA}$, $\epsilon_c = 0.119 \text{ \AA}$, and $\epsilon_u = 0.002$. We observe that all these parameters have a positive value, which indicates a downward bowing, being the lattice constant c which possesses the greatest deviation from the linear Vegard's law. This was experimentally reported by S. Yoshida *et al.* [11], and by Yun *et al.* [12]. Other works reported that the lattice parameters follow Vegard's law (see for example Angerer *et al.* [13]). From a theoretical approach, this alloy has only been studied using the virtual crystal approximation (VCA) by M. Goano *et al.* [14], and using first principles calculations by Z. Dridi *et al.* [15]. Furthermore, Liou *et al.* [16] have reported a non-linear behavior of the lattice parameters, although they found an upward bowing.

To compare our results with the available experimental data, we plot in Fig. 1a the calculated value of the c parameter together with the experimental results found in the literature [11]. As we can see, our calculated values follow the tendency shown by the experimental reports. Other examples of experimental studies for this alloy can be found in the works by D.K. Wickenden *et al.* [17], and K. Itoh *et al.* [18].

From our calculations we can obtain the nearest neighbor and the next nearest neighbor distances. Figure 2 compares our calculated distances with the experimental data of Refs. 19 and 20 for the $\text{Al}_{1-x}\text{Ga}_x\text{N}$ alloy. The experimental data are obtained from EXAFS (extend X-ray absorption fine structure) measurements. From the EXAFS technique the structure at local level can be investigated. This allows us to know the bond distance, the fraction of occupation, and the type of neighbors for a particular element. Figure 2 shows the good agreement between our calculated nearest and next nearest neighbor distances and the experimental data given in Refs. 19 and 20.

TABLE II. Structural parameters for the GaN, InN and $\text{In}_x\text{Ga}_{1-x}\text{N}$ alloys. The lattice parameters a and c are given in Å . For completeness we give the values for the GaN compound, already listed in Table I.

System	Parameter	This Work	Exp. Results	Other Calc.
GaN	a	3.2209	3.1890 ^a , 3.1892 ^b 3.1880 ^f , 3.19 ^f	3.1660 ^c , 3.189 ^d , 3.2000 ^e 3.1800 ^h , 3.1986 ⁱ , 3.17 ^j
	c	5.2368	5.1850 ^a , 5.185 ^b 5.18561 ^f , 5.189 ^g	5.1540 ^c , 5.185 ^d , 5.2200 ^e 5.1898 ^h , 5.2262 ⁱ , 5.151 ^j
	u	0.3780	0.3768 ^a , 0.377 ^g	0.3770 ^c , 0.3768 ^d , 0.3760 ^e 0.3760 ^h , 0.3772 ⁱ , 0.3768 ^j
$\text{In}_{0.25}\text{Ga}_{0.75}\text{N}$	a	3.3298		
	c	5.3987		
	u	0.3791		
$\text{In}_{0.50}\text{Ga}_{0.50}\text{N}$	a	3.4128		
	c	5.5257		
	u	0.3792		
$\text{In}_{0.75}\text{Ga}_{0.25}\text{N}$	a	3.4969		
	c	5.6333		
	u	0.3796		
InN	a	3.5440	3.5365 ^k , 3.5378 ^l 3.548 ^m , 3.540 ⁿ	3.520 ^c , 3.501 ^d , 3.480 ^e 3.525 ^h , 3.614 ⁱ , 3.546 ^j
	c	5.7228	5.7039 ^k , 5.7033 ^l 5.76 ^m , 5.705 ⁿ	5.675 ^c , 5.669 ^d , 5.64 ^e 5.68583 ^h , 5.8836 ⁱ , 5.7162 ^j
	u	0.3806		0.3799 ^c , 0.3784 ^d , 0.378 ^e 0.379 ^h , 0.37929 ⁱ , 0.379 ^j

^a Ref. 28 S. Strite *et al.*, ^b Ref. 29 T. Detchprohm *et al.*, ^c Ref. 15 Z. Dridi *et al.*, ^d Ref. 33 A.F. Wright *et al.*, ^e Ref. 34 C. Bungaro *et al.*,

^f Ref. 30 M. Leszczynski *et al.*, ^g Ref. 31 H. Schulz *et al.*, ^h Ref. 21 J. Serrano *et al.*, ⁱ Ref. 23 A. Zoroddu *et al.*, ^j Ref. 24 P. Carrier *et al.*,

^k Ref. 1 P. Yu. Davydov *et al.*, ^l Ref. 35 W. Paszkowicz *et al.*, ^m Ref. 36 T.L. Tansley *et al.*, ⁿ Ref. 37 K. Kubota *et al.*,

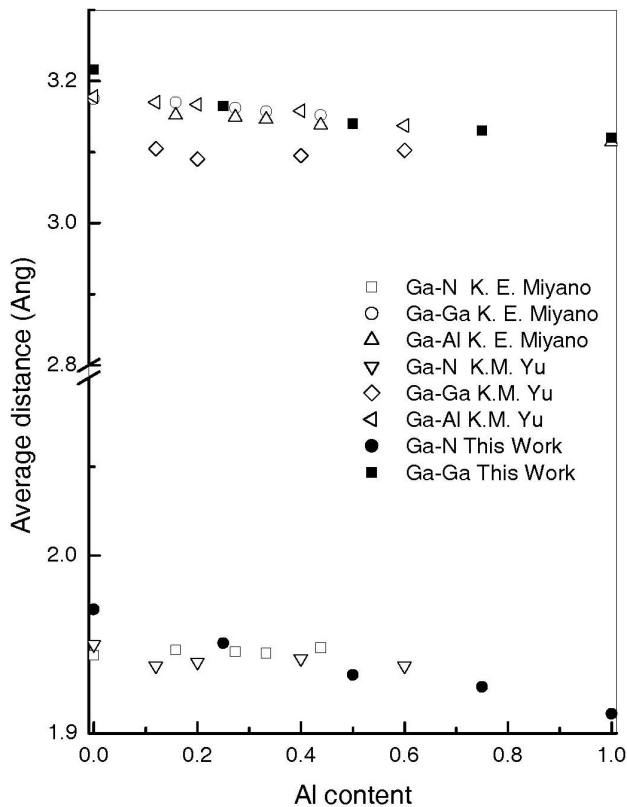


FIGURE 2. Comparison of the calculated and EXAFS data for the nearest and next nearest neighbor distances for $\text{Al}_{1-x}\text{Ga}_x\text{N}$. The experimental data, represented as empty points, are from Refs. 19 and 20, and the full points represent our calculated values.

3.1.2. $\text{In}_x\text{Ga}_{1-x}\text{N}$

The recent developments in blue–green optoelectronics are mainly due to the high efficiency luminescence of $\text{In}_x\text{Ga}_{1-x}\text{N}/\text{GaN}$ heterostructures. Despite their importance, several properties of $\text{In}_x\text{Ga}_{1-x}\text{N}$ alloys are not fully understood. For example, the optical properties of InN crystals are poorly known since the available growth techniques have not permitted the production of high quality epitaxial layers. Recent improvements in the molecular beam epitaxy (MBE) technique have led to the availability of high quality InN films. Photoluminescence measurements of these films indicate an energy gap around 1 eV or less [1]. The $\text{In}_x\text{Ga}_{1-x}\text{N}$ alloy has been studied theoretically by several groups using different methods. M. Goano *et al.* [14] used pseudopotentials to compute the gap through the virtual crystal approximation approach. Z. Dridi *et al.* [15] used LDA FP–LAPW and the virtual crystal approximation approach. J. Serrano *et al.* [21] worked within the framework of the density functional theory (DFT) with the local density approximation (LDA) using the Ceperley–Alder form for the exchange–correlation energy. C. Stampfl *et al.* [22] utilized the DFT, the LDA, and the GGA of Perdew *et al.* for the exchange–correlation functional. A. Zoroddu *et al.* [23] from first principles within the DFT utilized the plane-wave ultra-soft pseudopotential method within both the LDA and the

GGA. P. Carrier *et al.* [24] used plane-wave pseudopotentials and the LAPW method with the LDA.

In Table II we summarize our calculated structural parameters and compare them with some of the representative theoretical and experimental results found in the literature. From our results we can observe that the values of the a and c parameters increase when the In concentration increases. We plot these results in Fig. 1b. As in the previous case, there is not a linear dependence in these two parameters when the In concentration increases. If we adjust these results using Eq. (1), we obtain: $\epsilon_a = -0.140 \text{ \AA}$, $\epsilon_c = -0.188 \text{ \AA}$, and $\epsilon_u = 0.0001$. For this alloy we can observe that the deviation parameters for both a and c have a negative value, which implies an upward bowing as is clearly observed in Fig. 1b. This is not the case for the internal parameter, u , which has a nearly linear dependence with the In concentration as is demonstrated by the value of the bowing parameter, $\epsilon_u = 0.0001$. The simulation results indicate that the c lattice constant has a larger deviation from the linear Vegard’s law compared with the lattice constant a .

Figure 3 shows our calculated nearest and next nearest neighbor distances for $\text{In}_{1-x}\text{Ga}_x\text{N}$ and compares them with EXAFS measurements reported by T. Miyajima *et al.* [25]. Although the reported data are just for small values of the In –concentration (with the exception of two values for the

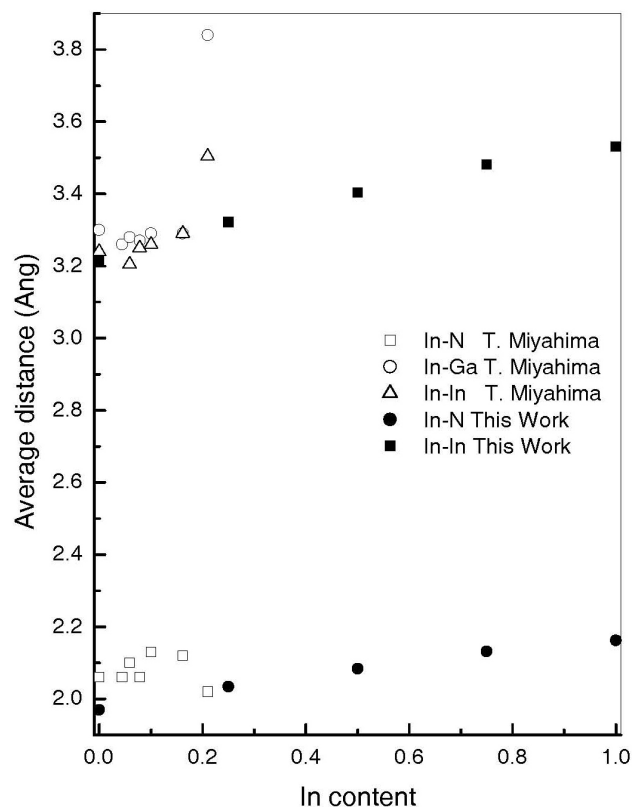


FIGURE 3. Comparison of the calculated and EXAFS data for the nearest and next nearest neighbor distances for $\text{In}_{1-x}\text{Ga}_x\text{N}$. The experimental data, represented as empty points, are from Ref. 26, and the full points represent our calculated values.

next nearest neighbor distances at the 20% of the In-concentration), we observe that our calculated values reproduce the experimental data.

T. Miyajima *et al.* [25] reported 3.22–3.30 Å and 3.25–3.30 Å, for the In – Ga and In – In distances respectively, and 1.85–2.21 Å for the In – N distance. In our calculations the values of the bond lengths In – Ga, and In – In for the interval of concentration $0 \leq x \leq 0.25$, are in the interval from 3.216–3.322 Å, whereas the nearest neighbor distance $d_{\text{In-N}}$ is in the interval 1.969–2.034 Å.

In a subsequent work, T. Miyajima *et al.* [26], using the EXAFS technique, measured the In – N and In – In distances in the InN compound and they obtained: $d_{\text{In-N}}=2.15$ Å and $d_{\text{In-In}}=3.53$ Å. Y. Nanishi *et al.* [27], using the EXAFS technique, measured these distances too, and they reported practically the same values ($d_{\text{In-N}}=2.14$ Å and $d_{\text{In-In}}=3.53$ Å). From our calculations, for the InN compound, we obtain the values: $d_{\text{In-N}}=2.162$ Å and $d_{\text{In-In}}=3.531$ Å. Therefore, from this quantitative comparison we observe that our calculations properly reproduce the experimental data.

Finally in Fig. 4, we plot the internal parameter, u , for both alloys as a function of the concentration x . Solid circles (squares) correspond to our results for $\text{Al}_x\text{Ga}_{1-x}\text{N}$ ($\text{In}_x\text{Ga}_{1-x}\text{N}$), and solid lines correspond to the fitting using Eq. (1).

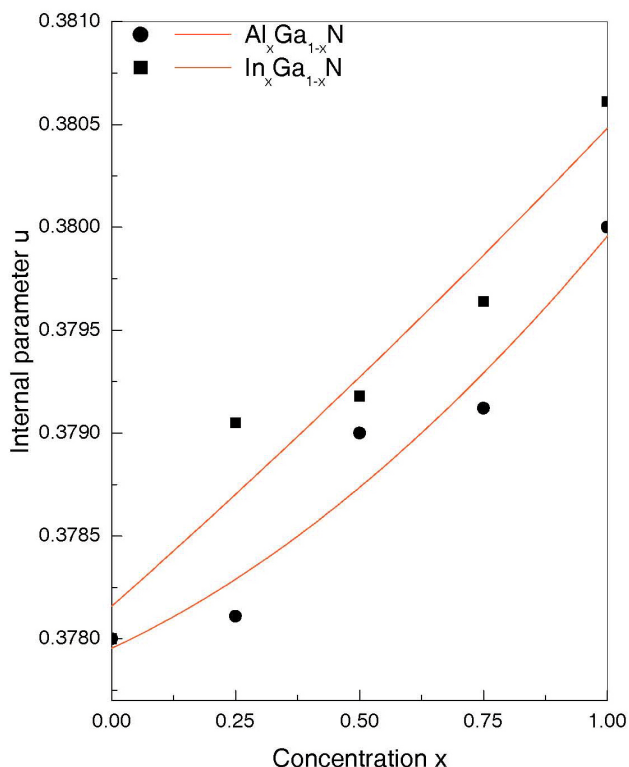


FIGURE 4. Internal parameter u for the $\text{Al}_x\text{Ga}_{1-x}\text{N}$ and $\text{In}_x\text{Ga}_{1-x}\text{N}$ alloys as a function of the Aluminium and Indium composition, x , respectively.

After comparing our calculated structural parameters with the experimental and theoretical results found in the literature for both alloys, we conclude that:

- 1) Our results for the binary compounds are in agreement with the published data, both experimental and theoretical.
- 2) For the $\text{Al}_x\text{Ga}_{1-x}\text{N}$ alloy, the structural parameters calculated in this work are in agreement with those reported in Ref. 11. For this alloy, the bowing parameters for a , c , and u , have positive values, indicating a downward bowing. This is in agreement with experimental and theoretical results reported previously.
- 3) For the $\text{In}_x\text{Ga}_{1-x}\text{N}$ alloy, the bowing parameter of the lattice constants a and c has a negative value, while the internal parameter u , has a positive value.
- 4) Our calculated values for the nearest neighbor and next nearest neighbor distances for both alloys are in good agreement with EXAFS data.

3.2. Electronic structure for the $\text{Al}_x\text{Ga}_{1-x}\text{N}$ and $\text{In}_x\text{Ga}_{1-x}\text{N}$ alloys

Before presenting our results of the electronic structure, we provide a summary of some representative theoretical and experimental results reported in the literature.

3.2.1. $\text{Al}_x\text{Ga}_{1-x}\text{N}$

Hagan *et al.* [38] and Baranov *et al.* [39] were the first to demonstrate experimentally the existence of the $\text{Al}_x\text{Ga}_{1-x}\text{N}$ alloy. Many other groups have measured its lattice constant, c , the optical bowing parameter, δ , and the energy gap as a function of the concentration. The magnitude of the optical bowing parameter accounts for the deviation of the band gap from the linear dependence. Using samples obtained by MBE, S. Yoshida *et al.* [11] measured the lattice constant c , and the band gap for the whole interval of concentrations ($0 < x < 1$). Comparing our results for this lattice constant with those reported by this author, there is very good agreement over the entire interval of concentrations. Although our calculated band gap value shows the experimental tendency reported by Yoshida *et al.* [11], we obtain slightly different values as can be seen in Fig. 5. However, other reported values for the band gap are well reproduced in our calculations (see Fig. 5). There are many experimental reports for this system obtained by different techniques and for different values of the concentration. In all these references there is no general agreement as to whether the fundamental parameters, *i.e.* the lattice constants and band gap, follow Vegard's law. Positive, negative, or small values of the optical bowing parameter can be found throughout the literature [2,11,17,18,40,41]. Theoretical results have been reported using the $\mathbf{k}\cdot\mathbf{p}$ method [43], the semi-empirical pseudopotentials method [14], *ab initio* LDA, DFT-LDA using molecular dynamics [42], and plane wave pseudopotentials using DFT-LDA [48].

TABLE III. Experimental and calculated values for the optical bowing parameter δ for $\text{Ga}_{1-x}\text{Al}_x\text{N}$ and $\text{Ga}_{1-x}\text{In}_x\text{N}$ alloys.

$\text{Ga}_{1-x}\text{Al}_x\text{N}$							
Method	δ [eV]	Method	δ [eV]	Method	δ [eV]	Method	δ [eV]
Exp. ^a	≈ 0	Exp. ^e	≈ 1	Theo. ^h	0.710	Theo. ^k	0.353
Exp. ^b	1	Exp. ^f	1	Theo. ⁱ	0.080	Theo. ^l	≈ 0
Exp. ^c	≈ 1	Exp. ^g	1.4	Theo. ^j	1.4000	Theo.*	0.0775
Exp. ^d	≈ 0						
$\text{Ga}_{1-x}\text{In}_x\text{N}$							
Method	δ [eV]	Method	δ [eV]	Method	δ [eV]	Method	δ [eV]
Exp. ^e	3.20	Exp. ^o	3.5	Theo. ^h	1.70	Theo. ^s	1.44
Exp. ^g	1.70	Exp. ^p	2.6	Theo. ⁱ	1.115	Theo.*	0.9990
Exp. ^m	2.50	Exp. ^q	1.4	Theo. ^r	0.1677		
Exp. ⁿ	1.00						

^a Ref. 11 S. Yoshida *et al.*, ^b Ref. 12 F. Yun *et al.*, ^c Ref. 78 K. Koide *et al.*, ^d Ref. 40 M.A. Khan *et al.*, ^e Ref. 41 T. Takeuchi *et al.*, ^f Ref. 44 O. Ambacher *et al.*, ^g Ref. 79 W. Walukiewicz *et al.*, ^h Ref. 15 Z. Dridi *et al.*, ⁱ Ref. 14 M. Goano *et al.*, ^j Ref. 42 K. Chen *et al.*, ^k Ref. 80 P. Y-K. Kuo *et al.*, ^l Ref. 43 S. K. Pugh *et al.*, ^m Ref. 1 Davydov *et al.*, ⁿ Ref. 45 S. Nakamura *et al.*, ^o Ref. 46 M. McCluskey *et al.*, ^p Ref. 47 C. Wetzel *et al.*, ^q Ref. 49 J. Wu *et al.*, ^r Ref. 33 A. F. Wright *et al.*, ^s Ref. 48 C. Caetano *et al.*, * Value calculated in this work.

TABLE IV. Band gap energy (in eV) for the $\text{Al}_x\text{Ga}_{1-x}\text{N}$ and $\text{In}_x\text{Ga}_{1-x}\text{N}$ alloys as a function of the concentration, x , obtained in the present work.

System	E_{gap} (eV)
GaN	1.768
$\text{Al}_{0.25}\text{Ga}_{0.75}\text{N}$	2.319
$\text{Al}_{0.50}\text{Ga}_{0.50}\text{N}$	2.830
$\text{Al}_{0.75}\text{Ga}_{0.25}\text{N}$	3.5123
AlN	4.027
GaN	1.768
$\text{In}_{0.25}\text{Ga}_{0.75}\text{N}$	1.088
$\text{In}_{0.50}\text{Ga}_{0.50}\text{N}$	0.871
$\text{In}_{0.75}\text{Ga}_{0.25}\text{N}$	0.489
InN	0.299

3.2.2. $\text{In}_x\text{Ga}_{1-x}\text{N}$

The first $\text{In}_x\text{Ga}_{1-x}\text{N}$ alloy with a high degree of ordering in layers grown on sapphire (0001) using metal-organic chemical vapor deposition (MOCVD) were obtained by Ruterana *et al.* [50]. Samples grown using different techniques and different concentrations have been studied, and authors report various values for the optical bowing parameter. Some of the representative results appear in Table III. In that table we summarize the theoretical and experimental results for the optical bowing parameter obtained from the literature for both alloys, together with the values obtained in this work. It can be seen from the table that there is a large discrepancy between the reported experimental and theoretical values. For theoretical calculations, most of the reported values are greater than one and they show a larger scattering in the

numerical values, especially in the case of the $\text{In}_x\text{Ga}_{1-x}\text{N}$ alloy.

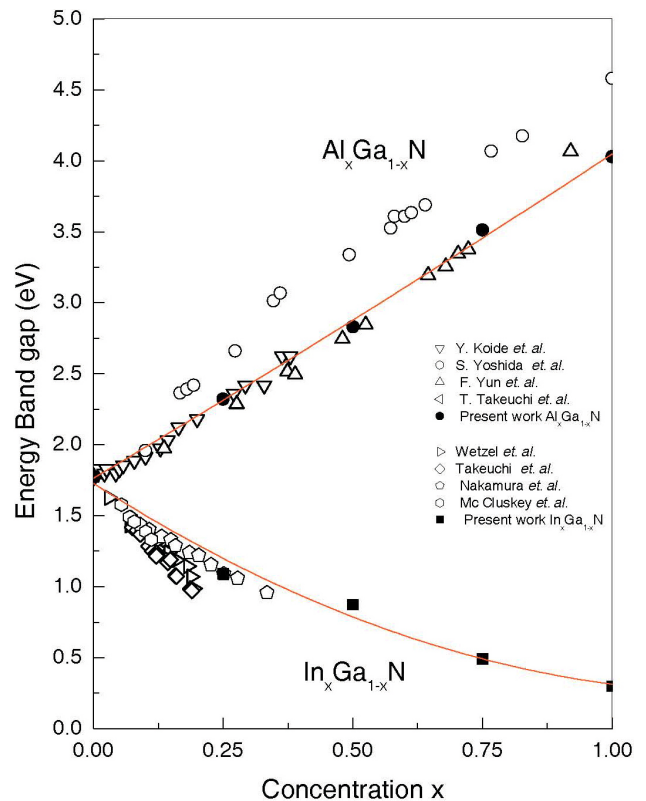


FIGURE 5. Variation of the band gap for the $\text{Al}_x\text{Ga}_{1-x}\text{N}$ and $\text{In}_x\text{Ga}_{1-x}\text{N}$ alloys as a function of the concentration, x . We present the experimental results from Table III and the solid lines represent the proposed adjustment to our results (solid points). For comparison we have rigidly moved downward the experimental data [77].

In Table IV we show the obtained results for the energy gap of the $\text{Al}_x\text{Ga}_{1-x}\text{N}$ and $\text{In}_x\text{Ga}_{1-x}\text{N}$ alloys from our *ab initio* calculations for different values of the concentration, x . These values correspond to 0, 25, 50, 75 and 100 % Al and In substitution. The plots corresponding to these data are displayed in Fig. 5. It can be seen that when the concentration of Al is increased the $\text{Al}_x\text{Ga}_{1-x}\text{N}$ alloy shows a nearly linear dependence. On the other hand, the $\text{In}_x\text{Ga}_{1-x}\text{N}$ alloy shows a non-linear dependence when we increase the In concentration. For both alloys we fit the gaps obtained by our calculations to a non-linear dependence using the quadratic phenomenological function [51]:

$$E_g(x) = xE_{g,A} + (1-x)E_{g,B} - \delta x(1-x), \quad (2)$$

where $E_{g,A}$ and $E_{g,B}$ correspond to the gap of the AlN (InN) and GaN for the $\text{Al}_x\text{Ga}_{1-x}\text{N}$ ($\text{In}_x\text{Ga}_{1-x}\text{N}$) alloy, and δ is the optical bowing parameter, which accounts for the non-linear behaviour of the band gap as a function of the concentration x . Substituting the values of Table IV into Eq. (2) we found $\delta = 0.3185$ and 0.9990 for $\text{Al}_x\text{Ga}_{1-x}\text{N}$ and $\text{In}_x\text{Ga}_{1-x}\text{N}$, respectively. The solid lines in Fig. 5 correspond to the non-linear fitting given by Eq. (2). As can be seen from the figure, there is a clear non-linear dependence for the $\text{In}_x\text{Ga}_{1-x}\text{N}$ alloy.

Concerning the electronic structure of these alloys, after comparing our results with those reported in the literature we conclude that:

1. For both alloys, most of the experimental results consider concentrations lower than $x=0.5$. This could account for the scattered values reported for the bowing parameter; however, experiments considering the whole interval of concentrations are better reproduced by our calculations.

2. The obtained value in this work for the bowing parameter ($\delta = 0.3185$) of the $\text{Al}_x\text{Ga}_{1-x}\text{N}$ alloy is in agreement with most of the experimental and theoretical results reported previously. Although many authors claim that the dependence on concentration of the band gap for this alloy should be linear ($\delta = 0.0$), it has become more accepted that there is a small deviation in the linear dependence.

3. For the $\text{In}_x\text{Ga}_{1-x}\text{N}$ alloy the reported results show a large scattering, especially in the experimental data. This has been partially explained in the literature as due to an inaccurate determination of the concentration. The quality of the samples and the measurement technique also play an important role in the determination of the optical bowing parameter. For this alloy, the scattering in the theoretical results reported in the literature is lower. Our calculations determined a value of $\delta = 0.9990$, which is in good agreement with those reported previously.

In Fig. 5 we show a comparison between our results and the experimental results reported for the band gap energy as a function of the concentration for the $\text{Al}_x\text{Ga}_{1-x}\text{N}$ and $\text{In}_x\text{Ga}_{1-x}\text{N}$ alloys. It can be seen from the figure that there is excellent agreement between them, especially for the $\text{Al}_x\text{Ga}_{1-x}\text{N}$ alloy. Most of the experimental data for the $\text{In}_x\text{Ga}_{1-x}\text{N}$ alloy are given for low concentrations of the In impurity. Nevertheless, our theoretical results follow the tendency demonstrated by experimental and theoretical results reported previously.

TABLE V. The electron and hole effective masses for AlN, GaN, InN and their alloys. All values are in units of the free-electron mass m_0 . For a recommended set of values for the binary compounds see Ref. 55.

		Present work			Other results			References
		m_e	m_h		m_e	m_h		
AlN	m^\perp	0.3012	4.3243	0.30 ^a	0.33 ^b	0.33 ^c	4.35 ^c	^a Ref. 55
	m^\parallel	0.2847	0.2427	0.32 ^a	0.32 ^b	0.32 ^c	0.28 ^c	^b Ref. 63
	m^*	0.2956	1.6528	0.31 ^d	0.48 ^e			^c Ref. 24
$\text{Al}_{0.75}\text{Ga}_{0.25}\text{N}$	m^\perp	0.2682	3.5247					^d Ref.61
	m^\parallel	0.2913	0.9325					^e Ref. 62
	m^*	0.2749	1.4743					^f Ref. 56
$\text{Al}_{0.50}\text{Ga}_{0.50}\text{N}$	m^\perp	0.2330	2.3039					^g Ref. 57
	m^\parallel	0.2411	0.5345					^h Ref. 59
	m^*	0.2427	1.2961					ⁱ Ref. 58
$\text{Al}_{0.25}\text{Ga}_{0.75}\text{N}$	m^\perp	0.2020	3.1232					^j Ref. 60
	m^\parallel	0.1958	0.1741					^k Ref. 62
	m^*	0.2000	1.1969					^l Ref. 67
GaN	m^\perp	0.1491	2.1072	0.20 ^a	0.21 ^b	0.22 ^c	0.39 ^c	^m Ref. 68
	m^\parallel	0.1803	2.1048	0.20 ^a	0.19 ^b	0.20 ^c	2.04 ^c	ⁿ Ref. 69

	m^*	0.1692	2.1412	0.22 ^f	0.23 ^g	0.20 ^h	2.2 ⁱ
				0.18 ^j	0.20 ^k	0.24 ^l	
				0.215 ^m			
$\text{In}_{0.25}\text{Ga}_{0.75}\text{N}$	m^\perp	0.1069	2.5409				
	m^\parallel	0.0968	2.4447				
	m^*	0.1035	2.4953				
$\text{In}_{0.50}\text{Ga}_{0.50}\text{N}$	m^\perp	0.1182	2.7958				
	m^\parallel	0.0921	2.6116				
	m^*	0.1025	2.8371				
$\text{In}_{0.75}\text{Ga}_{0.25}\text{N}$	m^\perp	0.0717	2.0304				
	m^\parallel	0.0623	2.1486				
	m^*	0.0781	2.2179				
InN	m^\perp	0.1299	1.9096	0.07 ^a	0.068 ^b	0.07 ^c	2.967 ⁿ
					0.068 ⁿ		
	m^\parallel	0.0892	2.2051	0.07 ^a	0.065 ^b	0.06 ^c	2.566 ⁿ
					0.072 ⁿ		
	m^*	0.1146	2.0301				

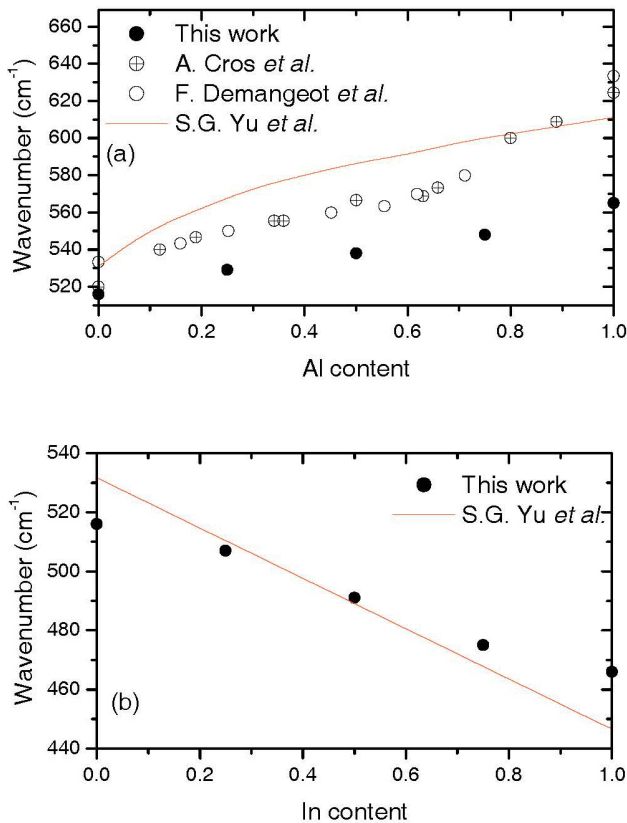


FIGURE 6. $A_1(TO)$ phonon dependence with Al concentration for $\text{Al}_x\text{Ga}_{1-x}\text{N}$ alloy (upper figure), and as a function of the In concentration for $\text{In}_x\text{Ga}_{1-x}\text{N}$ (lower figure). We present our calculations (full circles), the experimental results of Ref. 64 (open circles with plus), and Ref. 65 (open circles). Solid line depicts the calculated values from Ref. 66.

3.3. Calculated effective masses

As a by-product of our electronic band structure calculations, it is easy to compute the curvature of the minimum of the conduction band as well as the maximum of the valence band in the vicinity of the Γ -point. From these values the effective masses of the electrons and holes can be obtained.

At the Γ -point, the effective mass of the s -like conduction band can be obtained through a simple parabolic fit using the standard definition:

$$\frac{m_o}{m^*} = \frac{m_o}{\hbar^2} \frac{\partial^2 E}{\partial k^2} \quad (3)$$

with m^* the effective mass of the electrons and m_o the free electron mass.

The valence band states at the Γ -point are derived from the p -bonding states, and for the wurtzite crystals, these states are not as symmetric as those in the conduction band. However, we can calculate the curvature of the valence band maximum using the following approach: if the spin-orbit interaction were neglected, the top of the valence band would have a parabolic behavior. This implies that the highest valence bands are parabolic near the Γ -point. In this work, all the systems studied satisfy this parabolic condition of the maximum of the valence band at the Γ -point [52]. With this approach, and using Eq. (3), with the minus sign, we have calculated the effective masses of the heavy holes at the Γ -point.

Table V shows our calculated effective masses for the binary compounds, AlN, GaN, and InN, as well as for their related alloys. This table also includes theoretical and experimental values reported in the literature. The average effective mass can be obtained using

TABLE VI. Calculated $A_1(TO)$ mode for the different systems studied in this work. Comparison with other calculations and experimental data (all values in cm^{-1}).

System	Present work	Other results			Experimental	
GaN	516	537 ^a	545 ^b		533.8 ^c	533.5 ^d
Al ₂₅ Ga ₇₅ N	529					
Al ₅₀ Ga ₅₀ N	538					
Al ₂₅ Ga ₂₅ N	548					
AlN	565	649 ^a	615 ^c	619 ^e	613.8 ^c	
In ₂₅ Ga ₇₅ N	507					
In ₅₀ Ga ₅₀ N	491					
In ₇₅ Ga ₂₅ N	475					
InN	466	443 ^f			447 ^g	440 ^f

^a Ref. 70 I. Gorczyca *et al.*, ^b Ref. 71 M.R. Aouas *et al.*, ^c Ref. 72 Yu. Davidov *et al.*, ^d Ref. 73 J.M. Zhang *et al.*, ^e Ref. 74 K. Karch *et al.*,

^f Ref. 75 G. Kaczmarczyk *et al.*, ^g Ref. 76 Yu. Davidov *et al.*

$$m^* = [m_{\Gamma \rightarrow M}^{\perp} m_{\Gamma \rightarrow K}^{\perp} m_{\Gamma \rightarrow A}^{\parallel}]^{1/3}.$$

Where, m^{\perp} and m^{\parallel} are the masses in the direction perpendicular and parallel to the c -axis, respectively. For the binary compounds, we conclude that our calculated effective masses are in the range of most of the reported theoretical and experimental values. Moreover, our calculated values are in good agreement with those recommended by Vurgaftman and Meyer [55].

In the same table appear the effective masses for the alloys studied in this work. As we can see, the electron effective mass for $\text{Al}_x\text{Ga}_{1-x}\text{N}$ increases when we increase the Al concentration. To our knowledge, there are reports of the electron effective mass corresponding to the cubic phase only [53]. The behavior for our calculations and the reported cubic phase values show the same tendency, and this is also valid for the heavy hole effective mass. From Table V we can observe that the calculated effective masses for $\text{In}_x\text{Ga}_{1-x}\text{N}$ show a non-monotonic behavior as a function of the In concentration. The same behavior is observed in the cubic phase of this alloy, for intermediate values of the In concentration, reported in Ref. 54.

3.4. Zone center phonon calculation

Finally, and by using the so-called frozen phonon approach, we computed the zone center phonon modes, $A_1(TO)$ and $E_1(TO)$, considering the change of the total energy as a function of the displacement, u , of the atoms in the unit cell from their equilibrium positions. In particular, we can compute the $A_1(TO)$ mode by considering small displacements of the atoms along the optical axis (the c -axis) of the wurtzite phase. This is the only mode reported in this paper. In our approach we considered fixed the center of mass of the system, formed in this case by the cation (Al, Ga, In) and its nearest neighbor anion (N) [73]. Because we are at the minimum of the total

energy of the system, perturbation around this minimum allows us to use a parabolic approach to the total energy as a function of the displacement, *i.e.*,

$$E_{Total}(u) = E_o + uE_1 + u^2E_2 = \hbar\omega, \quad (4)$$

where E_i ($i = 0, 1, 2$) are fit parameters, and ω is the frequency. Within this approach, our calculated value for the $A_1(TO)$ mode for the binary compounds shows good agreement with most of the experimental reports as shown in Table VI. Figure 6a shows our calculated $A_1(TO)$ mode for the $\text{Al}_x\text{Ga}_{1-x}\text{N}$ alloy. In the same figure appear the experimental data of Refs. 64 and 65, and the theoretical calculations of Ref. 66. Although the numerical values are slightly different over the whole range of Al concentration, we obtain the same tendency than the experimental reports. On the other hand, Fig. 6b shows the $A_1(TO)$ mode for the $\text{In}_x\text{Ga}_{1-x}\text{N}$ alloy and we compare them with theoretical calculations reported in Ref. 66. As in the previous case, for the $A_1(TO)$ mode, we reproduce the tendency reported in Ref. 66. In conclusion, our calculations reproduce properly the reported values of the $A_1(TO)$ mode for the alloys as well as the corresponding binary compounds.

4. Conclusions

We have calculated the structural and electronic properties of wurtzite AlN, GaN, InN, and their related alloys, $\text{Al}_x\text{Ga}_{1-x}\text{N}$ and $\text{In}_x\text{Ga}_{1-x}\text{N}$. We found that, for both alloys, their structural parameters as a function of the concentration, x , do not follow Vegard's law. We observed that for the $\text{Al}_x\text{Ga}_{1-x}\text{N}$ alloy, the a , c , and u parameters have a positive bowing, with lattice constant c , the one that possesses the largest value. On the other hand, for the $\text{In}_x\text{Ga}_{1-x}\text{N}$ alloy, the a and c parameters have a negative bowing, while the bowing parameter for the internal parameter, u , is positive. Due to the good agreement between the nearest neighbor and next nearest neighbor distances obtained in this work, and the EXFAS measure-

ments, we can state that our calculation properly reproduces the structural properties. From our results of the electronic band structure calculations, we obtained the band gap as a function of the concentration, x , and characterized the deviation from the linear behavior calculating the optical bowing parameter, δ . We obtain a small optical bowing parameter, $\delta = 0.3185$, for the $\text{Al}_x\text{Ga}_{1-x}\text{N}$ alloy, which is consistent with results reported previously. The deviation from the linear behavior is more drastic for the $\text{In}_x\text{Ga}_{1-x}\text{N}$ alloy, due to the larger bowing parameter $\delta = 0.9990$, in accordance with most of the experimental results found in the literature. The effective masses of the systems studied in this work were calculated and the obtained values for the binary compounds, AlN, GaN, and InN, are in the range of those reported in the literature. To the best of our knowledge, this is the first time that the effective masses for these alloys have been reported. Finally, using the frozen phonon approach, we have com-

puted the $A_1(\text{TO})$ mode for the different systems studied in this work. We found good agreement with experimental values reported for the binary compounds; for the ternary alloys, we reproduce the experimental values for the $\text{Al}_x\text{Ga}_{1-x}\text{N}$ alloy, and the theoretical predictions for the $\text{In}_x\text{Ga}_{1-x}\text{N}$ alloy.

Acknowledgments

This work was done thanks to the Computer Facilities of IPICYT, San Luis Potosí, México. This work was partially supported by VIEP-BUAP under grant VIEP-BUAP 1/I/EXC/05, VIEP-BUAP 01/EXC/06-I. ELA acknowledges the assistance of CONACyT under grant No.165404. Part of this work was done during a research stay of DO at Freie Universität Berlin. DO greatly appreciates the hospitality of H. Kleinert, and gratefully acknowledges the financial support from CINVESTAV-IPN and CONACyT-México.

1. V. Yu. Davydov *et al.*, *Phys. Status Solidi B* **234** (2002) 787.
2. Y. Koide *et al.*, *J. Appl. Phys.* **61** (1987) 4540.
3. H. Morkoc *et al.*, *J. Appl. Phys.* **76** (1994) 1363.
4. J.I. Pankove, J.E. Berkeyheiser, H.P. Maruska, and J.P. Wittke, *J. Phys. Solid State Commun.* **8** (1970) 1051.
5. J.I. Pankove, *J. Lumin* **7** (1973) 114.
6. J. Wu *et al.*, *Applied Phys. Lett.* **80** (2002) 3967.
7. P. Hohenberg and W. Kohn, *Phys. Rev.* **136** (1964) 864; W. Kohn, L. Sham, *Phys. Rev. A* **140** (1965) 1133.
8. P. Blaha, K. Schwarz, G.K.H. Madsen, D. Kvasnicka, and J. Luitz, *WIEN2K*, An Augmented Plane Wave Plus Local Orbitals Program for Calculating Crystal Properties, ISBN 3-9501031-1-2, (Vienna University of Technology, Austria, 2001).
9. J.P. Perdew and Y. Wang, *Phys. Rev. B* **45** (1992) 13244; J.P. Perdew, K. Burke, and M. Ernzerhof, *Phys. Rev. Lett.* **77** (1996) 3865.
10. H.J. Monkhorst and J.D. Pack, *Phys. Rev. B* **13** (1976) 5188.
11. S. Yoshida, S. Misawa, and S. Gonda, *J. Appl. Phys.* **53** (1982) 6844.
12. F. Yun *et al.*, *J. Appl. Phys.* **92** (2002) 4837.
13. H. Angerer, *App. Phys. Lett.* **71** (1997) 1504.
14. M. Goano, E. Bellotti, E. Ghillino, G. Ghione, and K.F. Brennan, *J. Appl. Phys.* **88** (2000) 6476.
15. Z. Dridi, B. Bouhafs, and P. Ruterana, *Phys. Stat. Sol. (c)* **0** (2002) 315; Z. Dridi, B. Bouhafs, and P. Ruterana, *Semicond. Sci. and Technol.* **18** (2003) 850.
16. B.T. Liou, *Appl. Phys. A* **81** (2005) 1459.
17. D.K. Wickenden, C.B. Barger, W.A. Bryden, J. Miragliotta, and T.J. Kistenmacher, *Appl. Phys. Lett.* **65** (1994) 2024.
18. K. Itoh, T. Kawamoto, H. Amano, K. Hiramatsu, and I. Akasaki, *Jpn. J. Appl. Phys.* **30** (1991) 1924.
19. K.E. Miyano, J.C. Woicik, L.H. Robins, C.E. Bouldin, and D.K. Wickenden, *Appl. Phys. Lett.* **70** (1997) 2108.
20. Kin Man Yu *et al.*, *Appl. Phys. Lett.* **75** (1999) 4097.
21. J. Serrano and A. Rubio, *Phys. Rev. B* **62** (2000) 16612.
22. C. Stampfl and C.G. Van de Walle, *Phys. Rev. B* **59** (1999) 5521.
23. A. Zoroddu, F. Bernardini, P. Ruggerone, and V. Fiorentini, *Phys. Rev. B* **64** (2001) 045208.
24. P. Carrier and S. Wei, *J. Appl. Phys.* **97** (2005) 033707.
25. T. Miyajima *et al.*, *phys. stat. sol. (b)* **228** (2001) 45.
26. T. Miyajima *et al.*, *phys. stat. sol. (b)* **234** (2002) 801.
27. Y. Nanishi *et al.*, *phys. stat. sol. (a)* **200** (2003) 202.
28. S. Strite and H. Morkoç, *J. Vac. Sci. Technol. B* **10** (1992) 1237; and references therein.
29. T. Detchprohm, K. Hiramatsu, K. Itoh, and I. Akasaki, *Jpn. J. Appl. Phys. Part 2* **31** (1992) L1454.
30. M. Leszczynski *et al.*, *J. Appl. Phys.* **76** (1994) 4909.
31. H. Schulz and K.H. Thiemann, *Solid State Commun* **23** (1977) 815.
32. M. Tanaka, S. Nakahata, K. Sogabe, H. Nakata, and M. Tobioka, *Jpn. J. Appl. Phys.* **36** (1997) L1062.
33. A.F. Wright and J.S. Nelson, *Phys. Rev. B* **51** (1995) 7866.
34. C. Bungaro, K. Rapcewicz, and J. Bernholc, *Phys. Rev. B* **61** (2000) 6720.
35. W. Paszkowicz, *Powder Diffr.* **14** (1999) 258.
36. T.L. Tansley and C.P. Foley, *J. Appl. Phys.* **59** (1986) 3241.
37. K. Kubota, Y. Kobayashi, and K. Fujimoto, *J. Appl. Phys.* **66** (1989) 2984.
38. J. Hagan, R.D. Metcalfe, D. Wickenden, and W. Clark, *J. Phys. C* **11** (1978) L143.
39. B. Baranov *et al.*, *Phys. Status Solidi A* **49** (1978) G29.

40. M.A. Khan, R.A. Skogman, R.G. Schulze, and M. Gershenson, *Appl. Phys. Lett.* **43** (1983) 492.
41. T. Takeuchi *et al.*, *J. Appl. Phys.* **36** (1997) L177.
42. K. Chen and D.A. Drabold, *J. Appl. Phys.* **91** (2002) 9743.
43. S.K. Pugh, D.J. Dugdale, S. Brand, and R.A. Abram, *J. Appl. Phys.* **86** (1999) 3768.
44. O. Ambacher, *J. Phys. D: Appl. Phys.* **31** (1998) 2653.
45. S. Nakamura, *J. Vac. Sci. Technol. A* **13** (1995) 705.
46. M.D. McCluskey, C.G. Van de Walle, C.P. Master, L.T. Romano, and N.M. Johnson, *Appl. Phys. Lett.* **72** (1998) 2725.
47. C. Wetzel *et al.*, *Appl. Phys. Lett.* **73** (1998) 1994.
48. C. Caetano, L.K. Teles, M. Marques, A. Dal Pino, Jr., and L.G. Ferreira, *Phys. Rev. B* **74** (2006) 045215.
49. J. Wu *et al.*, *Phys. Stat. Sol. (b)* **240** (2003) 412.
50. P. Ruterana, G. Nouet, W. Van der Stricht, I. Moerman, and L. Considine, *Appl. Phys. Lett.* **72** (1988) 1743.
51. The quadratic behaviour of the band gap as a function of the composition was discussed experimentally by M. Cardona, *Phys. Rev.* **129** (1963) 69; S. Larach, R.E. Shrader, and C.F. Stocker, *Phys. Rev.* **108** (1957) 587. Theoretical interpretations were intended for R. Hill and D. Richardson, *J. Phys. C* **6** (1973) L115; D. Richardson, *J. Phys. C* **5** (1972) L27 ; and J.A. Van Vechten and T.K. Bergstresser, *Phys. Rev. B* **1** (1970) 3351.
52. See Figures 5.11–5.20 in E. López–Apreza, Ph. D. Thesis, BUAP, Puebla, Mexico (<http://www.fis.cinvestav.mx/~daniel/thELA.pdf>)
53. R. de Paiva, *et al.*, *Mat. Scie. and Engineering B* **93** (2002) 2.
54. K. Kassali and N. Bouarissa, *Solid–State Electronics* **44** (2000) 501.
55. I. Vurgaftman and J.R. Meyer, *J. Appl. Phys.* **94** (2003) 3675.
56. P. Perlin *et al.*, *Appl. Phys. Lett.* **68** (1996) 1114.
57. Y.J. Wang *et al.*, *J. Appl. Phys.* **79** (1996) 8007.
58. J.S. Im, A. Moritz, F. Steuber, V. Härle, F. Scholz, and A. Hangleiter, *Appl. Phys. Lett.* **70** (1997) 631.
59. S.K. O’Leary, B.E. Foutz, M.S. Shur, U.V. Bhapkar, and L.F. Eastman, *J. Appl. Phys.* **83** (1998) 826.
60. S. Elhamri, R.S. Newrock, D.B. Mast, M. Ahoujja, and W.C. Mitchel, *Phys. Rev. B* **57** (1998) 1374.
61. J.D. Albrecht, R.P. Wang, P.P. Ruden, M. Farahmand, and K.F. Brennan, *J. Appl. Phys.* **83** (1998) 1446.
62. B.E. Foutza, S.K. O’Leary, M.S. Shur, and L.F. Eastman *J. Appl. Phys.* **85** (1999) 7728.
63. P. Rinke *et al.*, *Phys. Rev. B* **77** (2008) 075202.
64. A. Cros *et al.*, *Solid State Comm.* **104** (1997) 35.
65. F. Demangeot *et al.*, *J. Appl. Phys.* **72**, (1998) 2674.
66. SeGi Yu, K.W. Kim, and L. Bergman, *Phys. Rev. B* **58** (1998) 15283.
67. T.Y. Lin *et al.*, *Phys. Rev. B* **58** (1998) 13793.
68. A. Saxler *et al.*, *J. Appl. Phys.* **87** (2000) 369.
69. D. Fritsch, H. Schmidt, and M. Grundmann, *Phys. Rev. B* **69** (2004) 165204.
70. I. Gorczyca, N.E. Christensen, E.L. Peltzer y Blanc, and C.O. Rodríguez, *Phys. Rev. B* **51** (1995) 11936.
71. M.R. Aouas, W. Sekkal, and A. Zaoui *Solid State Comm.* **120** (2001) 413.
72. V. Yu. Davydov *et al.*, *Phys. Rev. B* **58** (1998) 12899.
73. J.M. Zhang *et al.*, *Phys. Rev. B* **56** (1997) 14399.
74. K. Karch and F. Bechstedt *Phys. Rev. B* **56** (1997) 7404.
75. G. Kaczmarczyk *et al.*, *Appl. Phys. Lett.* **76** (2000) 2122.
76. V. Yu. Davydov *et al.*, *Appl. Phys. Lett.* **75** (1999) 3297.
77. Due to the band gap problem in *ab initio* calculations, and to reproduce optical properties, it is widely accepted to move rigidly the minimum of the conduction band. For more details see for example: G.A. Baraff and M. Schlüter, *Phys. Rev. B* **30** (1984) 3460; M.R. Pederson and B.M. Klein, *Phys. Rev. B* **37** (1988) 10319; F. Gygi and A. Baldereschi, *Phys. Rev. Lett.* **62** (1989) 2160; N. E. Christensen, in *High Pressure in Semiconductor Physics*, eds. T. Suski and W. Paul, Vol. 54 of *Semiconductors and Semimetals*, series eds. R.K. Willardson and E.R. Weber, (Academic Press, New York, 1998) p. 49, and references therein.
78. Y. Koide *et al.*, *J. Appl. Phys.* **61**, (1987) 4540.
79. W. Walukiewicz *et al.*, *J. Phys. D: Appl. Phys.* **39** (2006) R83.
80. Y–K. Kuo and W–W Lin, *Jap. J. of Appl. Phys. Part I* **41** (2002) 73.